Materials Transactions, Vol. 42, No. 8 (2001) pp. 1723 to 1730

Effects of Al, Si and Mo on Passivation Characteristics of Fe–10Cr Alloys *1

Katsuya Hio[1], Takashi Adachi[2, *2], Takashi Yamada[3], Yutaka Tsuchida[2], Koe Nakajima[2] and Yuzo Hosoi[2, *3]

[1]*Metals Laboratory, Industrial Research Division, Mie Prefectural Science and Technology Promotion Center, Kuwana 511-0937, Japan*
[2]*Department of Mechanical Engineering, Faculty of Engineering, Daido Institute of Technology, Nagoya 457-8530, Japan*
[3]*Inorganic Material Research Office, Materials Technology Department, Nagoya Municipal Industrial Research Institute, Nagoya 456-0058, Japan*

A study has been made on the effects of Al, Si and Mo on anodic polarization characteristics of Fe–10Cr alloys in 0.05–1.0 kmol·m^{-3} H_2SO_4 and NaCl solutions. Potential decay curves have also been measured in order to evaluate the stability of the passive films formed on Fe–10Cr alloys containing Al, Si and Mo. The analysis of the chemical composition of the passive film has been carried out by AES and XPS. The addition of Mo was very useful to decrease the critical passivation current density of Fe–10Cr alloys which contained Al and Si. The passive current density decreased with addition of 2 mass%Mo to Fe–10Cr–3Si alloy, while it increased in Fe–10Cr–3Al alloy. Pitting potential was moved toward the noble direction by the addition of Mo, except for the case of Fe–10Cr–3Al–3Si–2Mo alloy. It seems that Laves phase (Fe_2Mo) was precipitated in this alloy, and Mo-depleted zone was formed locally. The potential decay time of the passive film was increased by the addition of Al, Si and Mo to Fe–10Cr alloys. Two step potential decay curves were obtained in Si-containing alloys, and this behavior of the decay curve was shown more clearly in Fe–10Cr–3Si–2Mo alloy. The results of AES and XPS analysis indicated that Cr and Al concentrated in the passive film of Fe–10Cr–Al alloy. In the case of Fe–10Cr–Si alloy, Si concentrated in the surface region of the film and Cr in the internal region of the film. The confirmation was not possible for the enrichment of Mo in the passive film.

(Received February 2, 2001; Accepted June 6, 2001)

Keywords: *iron-chromium alloy, aluminum, silicon, molybdenum, anodic polarization, pitting potential, decay curve, passive film, Auger electron spectroscopy, x-ray photoelectron spectroscopy*

1. Introduction

The possibility of the development of Cr-saving ferritic stainless steel in which a part of Cr is substituted by Al and/or Si was presented in our previous papers.[1,2] It was found that alloying of 3 mass% (%) Al or 3%Si to Fe–10Cr alloy was very beneficial in improving passivating characteristics and pitting resistance, which were comparable or better than those of 12%Cr stainless steel.

Mo is well known as a very effective alloying element to improve the corrosion resistance especially to increase the pitting corrosion resistance of stainless steels.[3,4] Most of the research on the effect of Mo on corrosion resistance has been directed to relatively high Cr steels such as 19Cr–2Mo in ferritic stainless steels.[5–7] However, very little work is available on the low Cr steels under 12%Cr. It is worthwhile to discuss the effect of Mo on the corrosion resistance of the Cr-saving ferritic stainless steel in terms of technology, although Mo is valuable metal to be conserved the resources.

A large number of researches[8–10] have been carried out on the passivation phenomena of metals and alloys. The passive film of the stainless steel is usually very thin about 1–5 nm in thickness,[11] and Cr is concentrated in the film.[12–14] The corrosion resistance is maintained by the protective effect of hydration Cr oxide and Cr oxyhydroxide film.[15,16] In Fe–10Cr alloy, the formation of passive film is considered to be imperfect because of insufficient Cr content to produce protective Cr compounds. Therefore, it becomes notable whether the addition of Al, Si and Mo enables the reinforcement of the passive film.

A study was made on the effect of Al, Si and Mo on the anodic polarization and pitting corrosion of Fe–10Cr alloys with Al and Si in H_2SO_4 and NaCl aqueous solutions. The measurement of the potential decay curve was also done to evaluate the stability of the passive film by the addition of the alloying elements. In addition, the chemical composition of the passive film was analyzed by Auger electron spectroscopy (AES) and X-ray photoelectron spectroscopy (XPS).

2. Experimental Procedures

The alloys were prepared by vacuum arc melting as button ingot from electrolytic iron, ferrochrome, pure aluminum, metallic silicon and metallic molybdenum. These button ingots of about 200 g weight were hot-pressed at 1473 K into about 4 mm thick plates, then annealed at 1073 K for 1.8 ks. Chemical compositions of the alloys are listed in Table 1. Specimens for the electrochemical measurement were cut into a plate of 10 mm × 10 mm and embedded in epoxy resin. These specimens were mirror-finished with alumina suspension. Ultrasonic cleaning was carried out in pure water.

Potentiodynamic anodic polarization curve was measured on each alloy from the corrosion potential at a sweep rate of 1 mV·s^{-1} in 0.05–1 kmol·m^{-3} H_2SO_4 solution. The potential was measured with respect to a saturated calomel electrode (SCE), and Pt was used as a counter electrode. Prior to the polarization curve measurement, a specimen was cathodically polarized at −0.7 V for 0.6 ks, then kept at an open circuit potential for 0.6 ks. Pitting potential of various alloys was es-

*1 This Paper was Originally Published in Japanese in J. Japan Inst. Metals, **64** (2000) 1148–1155.
*2 Graduate Student, Daido Institute of Technology. Present address: Aikoku Alpha Co., Ltd.
*3 Present address: Professor Emeritus, Nagoya University and Daido Institute of Technology.

Table 1 Chemical composition of Fe–10Cr alloys.

(mass%)

Samples	C	Cr	Al	Si	Mo	Fe
Fe–10Cr	0.003	10.00	< 0.01	< 0.01	< 0.01	Balance
Fe–10Cr–3Al	0.007	10.06	2.94	< 0.01	< 0.01	Balance
Fe–10Cr–3Al–1Mo	0.005	10.05	2.98	< 0.01	1.04	Balance
Fe–10Cr–3Al–2Mo	0.005	10.05	2.98	< 0.01	2.07	Balance
Fe–10Cr–3Si	0.005	10.03	< 0.01	2.88	< 0.01	Balance
Fe–10Cr–2Mo	0.002	10.04	< 0.01	< 0.01	2.00	Balance
Fe–10Cr–3Si–2Mo	0.004	10.05	< 0.01	2.96	2.03	Balance
Fe–10Cr–3Al–3Si	0.007	10.07	2.96	2.98	< 0.01	Balance
Fe–10Cr–3Al–3Si–1Mo	0.008	10.06	3.06	3.00	1.04	Balance
Fe–10C–3Al–3Si–2Mo	0.004	10.05	3.06	2.96	2.03	Balance
Fe–10Cr–5Al	0.008	10.04	4.96	< 0.01	< 0.01	Balance
Fe–10Cr–5Si	0.006	10.02	< 0.01	4.84	< 0.01	Balance

timated in 3.5% and 0.05–1 kmol·m^{-3} NaCl solution. Specimens were immersed in the solution for 0.6 ks, then polarized from the corrosion potential at a sweep rate of 0.33 mV·s^{-1}. The potential at which the current density reached at 1 A·m^{-2} was taken as the pitting potential. H_2SO_4 and NaCl aqueous solutions were deaerated by bubbling N_2 gas for 1.8 ks, followed by continuous purging during the above-mentioned tests. Temperature of the solutions was held at 303 K.

The time to breakdown passive film was measured in 0.05 kmol·m^{-3} H_2SO_4 solution deaerated by N_2 gas at 300 K. The specimen was polarized at 0.75 V for 0.3 ks to form passive film. After that, the circuit was open, and the passive film began to deteriorate, which gradually decreased the potential. The change in the potential with this destruction of the passive film was recorded.

The composition in the depth direction of a passive film of Fe–10Cr alloys containing Al, Si or Mo was analyzed by an Auger electron spectrometer (AES) and X-ray photoelectron spectroscopy (XPS). The AES analysis was made in the integration mode. The Auger peaks recorded were Fe (LM2), Cr (LM2), Al (KL1), Si (KL1), Mo (MN2) and O (KL1). The content of each element was determined quantitatively by multiplying the intensity of each peak by the relative sensitivity factor. The acceleration voltage and the current of the primary electron beam were 10 kV and 30 nA, respectively. The acceleration voltage and the current of the Ar^+ sputtering beam were 3 kV and 1.5 μA, respectively. Ar^+ sputtering rate was equivalent to 0.083 nm·s^{-1} in SiO_2. On the other hand, in the XPS spectrometer an Al–Kα X-ray source was used with the acceleration voltage of 15 kV and the emission current of 20 mA. The Ar^+ sputtering beam was similarly with the AES analysis, and Ar^+ sputtering rate was equivalent to 0.017 nm·s^{-1} in SiO_2. For both the AES and XPS analyses, the background pressure in the test chamber was 5×10^{-8} Pa, and was 4×10^{-5} Pa after high-pure Ar gas was introduced for sputtering. The specimens for these analyses were polished using No. 1200 emery paper with water, degreased in acetone, and passivated in 30%HNO_3 solution at 303 K for 3.6 ks.

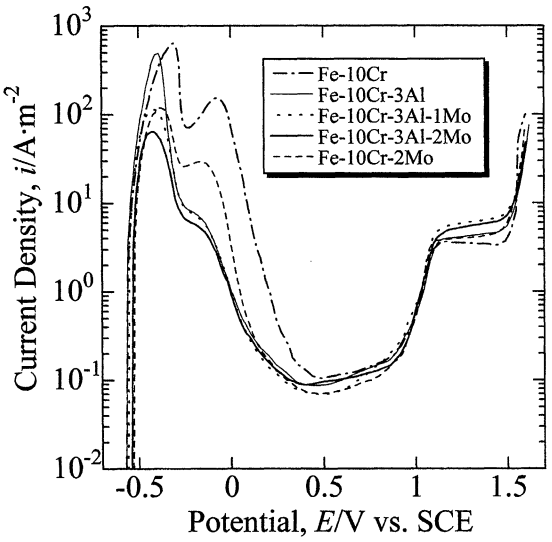

Fig. 1 Effects of Al and Mo on the anodic polarization curves of Fe–10Cr alloys in 0.5 kmol·m^{-3} H_2SO_4 solution at 303 K.

3. Results and Discussion

3.1 Anodic polarization curve and pitting potential

The effect of Al and Mo on the anodic polarization curves of Fe–10Cr alloys in 0.5 kmol·m^{-3} H_2SO_4 solution is shown in Fig. 1. It is indicated that the addition of Mo decreased the critical passivation current density (i_{crit}) of Fe–10Cr alloys. It should be noted that this beneficial effect of Mo was also presented in relatively low Cr steels, as well as high Cr steels.[17,18] The second peak observed at the high-potential side in the active region of Fe–10Cr alloys as reported in the previous paper[2] is again observed in the Fe–10Cr–2Mo alloy. The addition of Mo has no effect to suppress the second dissolution, which is known as the selective dissolution of Fe.[19] The passive current density (i_{pass}) of the Fe–10Cr–3Al alloy was decreased by the addition of 1%Mo, but it maintained a similar i_{pass} value by the addition of 2%Mo. About the same i_{pass} values were observed in both the Fe–10Cr–3Al–1Mo and Fe–10Cr–2Mo alloys. Here, the lowest current density observed in the passive region is designated as the i_{pass} value.

The effect of Al and Mo on the anodic polarization curves of Fe–10Cr–3Si alloys in 0.5 kmol·m^{-3} H_2SO_4 solution is in-

dicated in Fig. 2. The addition of 2%Mo to the Fe–10Cr–3Si alloy or 1%Mo to the Fe–10Cr–3Al–3Si alloy results in the decrease of the i_{crit} to nearly the same level. On the contrary, the i_{pass} of Fe–10Cr–3Si alloys seems to be increased by the addition of Mo and Al. A rapid increase of the current density in the transpassive region was induced by the action of Si, and the addition of Mo enhanced this tendency.

In Fig. 3, the relationship between the concentration of H_2SO_4 ($C_{H_2SO_4}$) and the i_{crit} value is plotted on a log scale. It is confirmed that the linear relationship was obtained between these two values. The following equations were derived for each alloy.

Fe–10Cr–3Al–1Mo

$$\log(i_{crit}) = 0.49\log(C_{H_2SO_4}) + 2.2 \quad (1)$$

Fe–10Cr–3Al–2Mo

$$\log(i_{crit}) = 0.47\log(C_{H_2SO_4}) + 2.0 \quad (2)$$

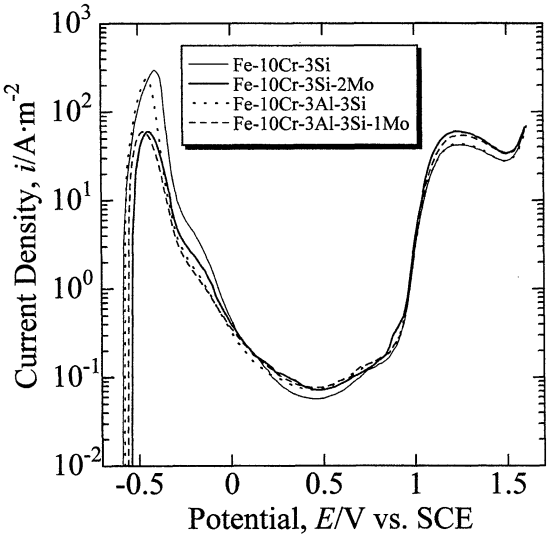

Fig. 2 Effects of Al and Mo on the anodic polarization curves of Fe–10Cr–3Si alloys in 0.5 kmol·m^{-3} H_2SO_4 solution at 303 K.

Fe–10Cr–3Si–2Mo

$$\log(i_{crit}) = 0.46\log(C_{H_2SO_4}) + 1.9 \quad (3)$$

Fe–10Cr–3Al–3Si–1Mo

$$\log(i_{crit}) = 0.46\log(C_{H_2SO_4}) + 1.9 \quad (4)$$

Fe–10Cr–2Mo

$$\log(i_{crit}) = 0.49\log(C_{H_2SO_4}) + 2.2 \quad (5)$$

It is noted that the gradient (the dependence of H_2SO_4 concentration) of each alloy became nearly equal by the alloying of Mo. This gradient of Fe–10Cr alloy, as previously reported,[2] was changed by the addition of Al and Si, as shown in the following equations.

Fe–10Cr

$$\log(i_{crit}) = 0.68\log(C_{H_2SO_4}) + 3.1 \quad (6)$$

Fe–10Cr–3Al

$$\log(i_{crit}) = 0.88\log(C_{H_2SO_4}) + 3.0 \quad (7)$$

Fe–10Cr–3Si

$$\log(i_{crit}) = 0.71\log(C_{H_2SO_4}) + 2.7 \quad (8)$$

Fe–10Cr–3Al–3Si

$$\log(i_{crit}) = 0.69\log(C_{H_2SO_4}) + 2.6 \quad (9)$$

That is to say, the alloying of Mo is effective to reduce the dependence of the i_{crit} upon the H_2SO_4 concentration in the Fe–10Cr–Al and Fe–10Cr–Si alloy system.

Figure 4 shows the effects of the H_2SO_4 concentration on the i_{pass} for various alloys in terms of the relationship between log ($C_{H_2SO_4}$) and log (i_{pass}). The i_{pass} value of alloys tested increased linearly with increasing H_2SO_4 concentration except the Fe–10Cr–3Al–2Mo alloy. The rate of increase in i_{pass} became larger as the H_2SO_4 concentration increased for the Fe–10Cr–3Al–2Mo alloy. With respect to the dissolution of Mo in aqueous solutions, it was dissolved as Mo(VI) ion regardless of the kind of aqueous solutions,[20,21] and Nakamura and Haruyama[22] pointed out that Mo in 0.5 kmol·m^{-3} H_2SO_4

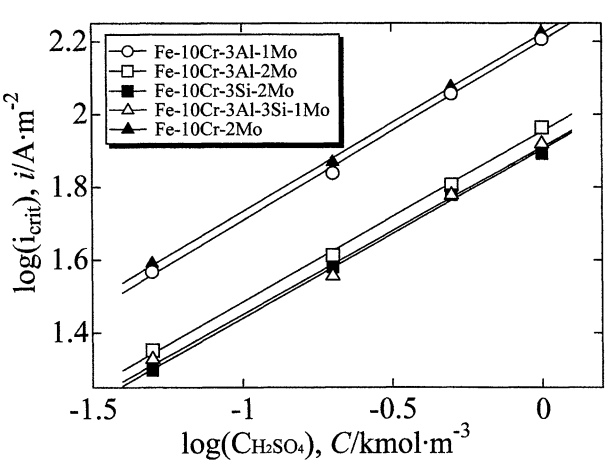

Fig. 3 Relationship between the concentration of H_2SO_4 and the critical passivation current density for Fe–10Cr–3Al–1Mo, Fe–10Cr–3Al–2Mo, Fe–10Cr–3Si–2Mo, Fe–10C–3Al–3Si–1Mo and Fe–10Cr–2Mo alloys in H_2SO_4 aqueous solution at 303 K.

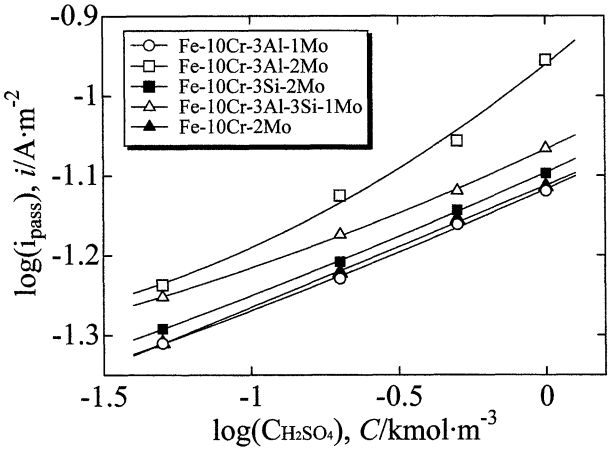

Fig. 4 Relationship between the concentration of H_2SO_4 and the passive current density of Fe–10Cr–3Al–1Mo, Fe–10Cr–3Al–2Mo, Fe–10Cr–3Si–2Mo, Fe–10Cr–3Al–3Si–1Mo and Fe–10Cr–2Mo alloys in H_2SO_4 aqueous solution at 303 K.

solution was dissolved as $HMoO_4^-$. In the present study, Mo is considered to be dissolved as $HMoO_4^-$ in a passive region of the Fe–10Cr–3Al–2Mo alloy, resulting in the increase of current density. However, the role of Al to accelerate the dissolution of Mo is not clear, and it should be clarified in a further investigation. In addition, these tendencies were not observed when 2%Mo was added to the Fe–10Cr–3Si alloy. In this case, the observed relationship was similar to that in the Fe–10Cr–2Mo alloy. These results suggest that Si does not affect the dissolution of Mo.

The pitting potential of each alloy in 3.5%NaCl solution is summarized in Fig. 5. The combination of alloying of Al with Mo to Fe–10Cr alloy was useful to move pitting potential to noble direction, and the addition of Si and Mo was more effective to obtain higher pitting potential. The pitting potential was reached to the most noble value by combined addition of Al, Si and Mo to Fe–10Cr (Fe–10Cr–3Al–3Si–1Mo) alloy. The reason why the pitting potential increases with the addition of Mo in NaCl aqueous solution is considered to be as follows. Mo dissolves as MoO_4^{2-} and forms a selective layer of anions at the outermost layer of the passive film, which suppresses the attack of Cl^- ions,[23,24] resulting in the increase of corrosion-suppression effect. Conversely, the pitting potential of Fe–10Cr–3Al–3Si alloy was decreased by 2%Mo because of the formation of Laves phase, discussed later.

The effect of the NaCl concentration on the pitting potential is shown in Fig. 6. Generally, there is the following relation between the concentration of anion and pitting potential.[25]

$$E_{pit} = A - B\log(C_{X^-}) \tag{10}$$

E_{pit} is pitting potential in halide ion X^-, C_{X^-} is concentration of X^-, and A and B are constants. The relationship between the pitting potential and the Cl^- concentration in each alloy is expressed as the following equation in this experiment.

Fe–10Cr–3Al–1Mo

$$E_{pit} = -0.095 - 0.26\log(C_{Cl^-}) \tag{11}$$

Fe–10Cr–3Al–2Mo

$$E_{pit} = -0.078 - 0.27\log(C_{Cl^-}) \tag{12}$$

Fe–10Cr–3Si–2Mo

$$E_{pit} = +0.14 - 0.24\log(C_{Cl^-}) \tag{13}$$

Fe–10Cr–3Al–3Si–1Mo

$$E_{pit} = +0.078 - 0.21\log(C_{Cl^-}) \tag{14}$$

Fe–10Cr–2Mo

$$E_{pit} = -0.10 - 0.26\log(C_{Cl^-}) \tag{15}$$

The relationship between the pitting potential and the Cl^- concentration of the Fe–18Cr–8Ni alloy in NaCl aqueous solution has been presented by Shiobara and Morioka[26] as follows.

$$E_{pit} = +0.48 - 0.22\log(C_{Cl^-}) \tag{16}$$

The gradient of C_{Cl^-} dependence for Fe–10Cr–3Si–2Mo and Fe–10Cr–3Al–3Si–1Mo alloys which showed excellent corrosion resistance was comparable with that of the eq. (16). It is considered that combined addition of Al, Si and Mo of proper quantity to Fe–10Cr alloy has similar effect on the combination alloying of 18Cr with 8Ni to Fe base in the pitting corrosion behavior in NaCl aqueous solution. Further investigation should be needed to make clear the role of combined addition of Al, Si and Mo in the pitting corrosion resistance from this point of view.

3.2 Potential decay curve

Figure 7 indicates the potential decay curves of alloys tested. The potential decay time of the passive film formed on the Fe–10Cr alloy was prolonged by the addition of 3%Al. The potential decay was prolonged further by the addition of 3%Si, and modified into a two-step process. The addition of Mo was effective in increasing the potential decay time of the Fe–10Cr–3Al and also the Fe–10Cr–3Si alloy, and changed the decay into two-step process. The decay time of the second step was extremely prolonged in the Fe–10Cr–3Si–2Mo alloy. The tendency of two-step decay was also observed in the Fe–10Cr–2Mo alloy, in which only Mo was added. It is suggested from these results that there is a difference of the structural characteristics of passive film between the Fe–10Cr–Si

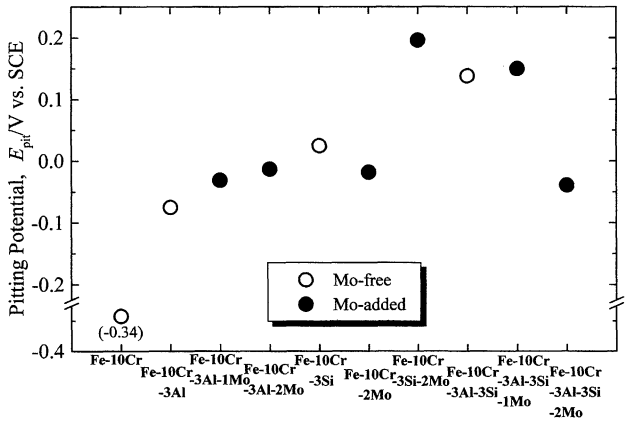

Fig. 5 Effects of Al, Si and Mo on the pitting potential of Fe–10Cr alloys in 3.5 mass%NaCl solution at 303 K.

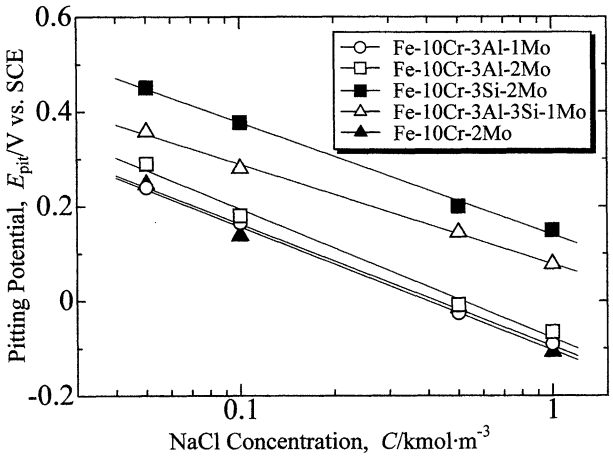

Fig. 6 Relationship between the concentration of NaCl and the pitting potential of Fe–10Cr–3Al–1Mo, Fe–10Cr–3Al–2Mo, Fe–10Cr–3Si–2Mo, Fe–10C–3Al–3Si–1Mo and Fe–10Cr–2Mo alloys in NaCl aqueous solution at 303 K.

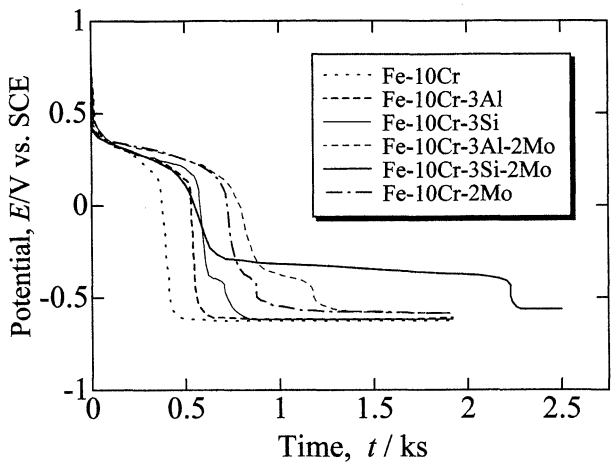

Fig. 7 The potential decay curves after passivation at 0.75 V (vs. SCE) for 0.3 ks in 0.05 kmol·m^{-3} H_2SO_4 solution at 300 K.

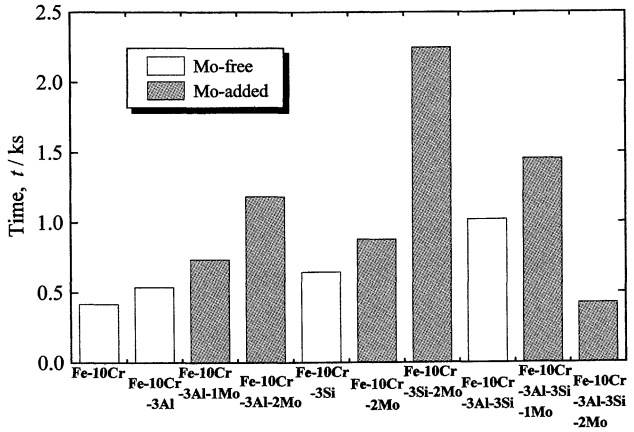

Fig. 8 Effects of Al, Si and Mo on the potential decay time of Fe–10Cr alloys passivated at 0.75 V (vs. SCE) for 0.3 ks in 0.05 kmol·m^{-3} H_2SO_4 solution at 300 K.

or –Mo alloy and the Fe–10Cr–Al alloy.

Figure 8 illustrates the potential decay times of passive films on various alloys obtained from the results of the potential decay curves. The potential decay time of passive film was prolonged when Mo was added to the Fe–10Cr–3Al or Fe–10Cr–3Si alloy. The best film stability was obtained in the Fe–10Cr–3Si–2Mo alloy as shown in Fig. 8. In the case of Fe–10Cr–3Al–3Si alloy, however, addition of 1%Mo prolonged the potential decay time, but conversely, it was shortened by the addition of 2%Mo. This tendency is similar to the results of pitting potential described before. To make clear the effect of Mo, the alloy phase and microstructure were examined. Figure 9 shows a phase diagram of the Fe–10Cr–3Al–3Si–xMo system which was obtained using integrated thermodynamics calculation software (Thermo-Calc: Royal Institute of Technology).[27] The region of precipitation of Laves phase (Fe_2Mo) extends to high-temperature side and the precipitation is easy to occur as the Mo content increases. Figure 10 shows the EPMA observation of the Fe–10Cr–3Al–3Si–2Mo alloy. In the SEM image, precipitates of 1 μm in size were observed along the grain boundaries. Since Mo was detected in these precipitates and taking the phase diagram shown in Fig. 9 into consideration, these precipitates are thought to be the Laves phase of Fe_2Mo. The inhomogeneous nature of these precipitates as well as the consumption of Mo is speculated to cause the deterioration of the corrosion resistance of the Fe–10Cr–3Al–3Si–2Mo alloy. Iseda *et al.*[28] reported that the solubility limit of Mo decreases with increasing Si content in 9Cr–2Mo steel. Miyahara *et al.*[29] also mentioned that an increase in the Si content promoted the precipitation of the Laves phase in Fe–10Cr–Mo alloy. In the present study, the role of Al must be also considered in the precipitation of Laves phase. The corrosion resistance increased when 2%Mo was added to the Fe–10Cr–3Si alloy, but it deteriorated when 2%Mo was added to the Fe–10Cr–3Al–3Si alloy. This deterioration was supposed to be due to the precipitation of the Laves phase. Whether or not Al (in addition to Si) is involved in the precipitation of the Laves phase is an issue that remains to be solved in the future in these alloy system.

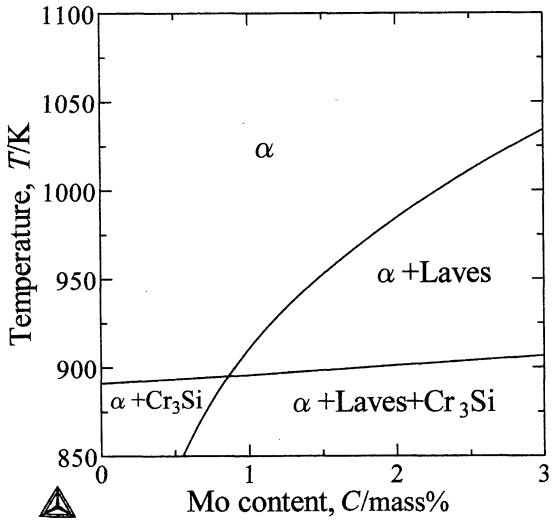

Fig. 9 Phase diagram of Fe–10Cr–3Al–3Si–xMo alloy system.

3.3 Analysis of passive film

The chemical compositions of passive film were analyzed with AES for the Fe–10Cr–5Al and Fe–10Cr–5Si alloys in which the Al or Si content was relatively high because of the convenience of analysis of the thin film. The concentrated Cr and Al were observed on the most surface layer in the passive film of Al-added alloy as shown in Fig. 11. In contrast, a large amount of Si concentrated on the surface and Cr concentrated in shallow interior region in the Si-added alloy. The concentration of Mo in the passive film was not confirmed in the Mo-added alloy by AES analysis. With respect to Mo in a passive film in stainless steel, the presence was also hardly observed by AES in the previous papers.[4,30,31] Figure 12 shows the chemical shifts in the kinetic energy of the Auger electrons of the Al or Si ion in the depth direction. The peaks in the kinetic energy of pure Al and Al_2O_3 were measured at 1398 eV and 1390 eV, respectively. Up to a sputtering time of 60 s, the peak of the kinetic energy of Al for the Fe–10Cr–5Al alloy exhibited a value similar to that of Al_2O_3. At periods after 60 s, it became constant and closer to that of pure Al, suggesting that chemical compounds of Al were formed at the surface. As for pure Si and SiO_2, their peaks of kinetic energy were measured at 1622 eV and 1612 eV, respectively. The peak of the kinetic

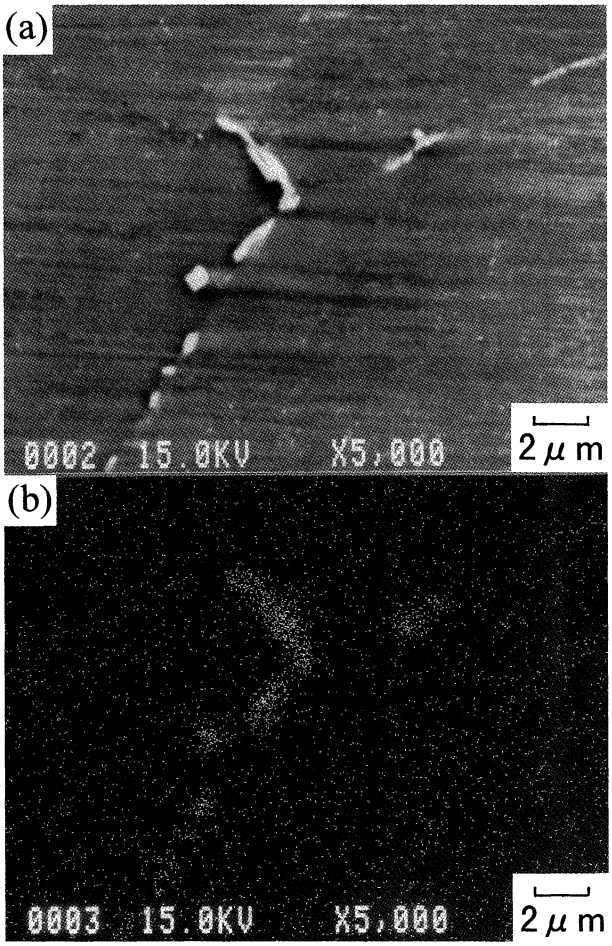

Fig. 10 A SEM image (a) and a Mo map (b) obtained by EPMA analysis of Fe–10Cr–3Al–3Si–2Mo alloy.

energy of Si for the Fe–10Cr–5Si alloy was observed at the value similar to that of SiO_2 near the surface, and it closed to that of pure Si after sputtering for 20 s or longer. These results suggest that Si compound would be formed at the surface.

Figure 13 shows the results of XPS analyses for Al, Si, Cr and Mo in the passive films of Fe–10Cr–3Al, Fe–10Cr–3Si and Fe–10Cr–2Mo alloys. In the Al 2p spectrum of the passive film of Fe–10Cr–3Al alloy, a main peak was positioned at approximately 75 eV on the surface of the passive film, which may correspond to the peak of Al^{3+}.[32] In addition, a peak corresponding to the metallic state was observed at approximately 72.9 eV.[33] After sputtering the passive film for 270 s by Ar ions, the value of the peak for metallic state increased and the value of the peak at 75 eV decreased. In the Si 2p spectrum of the passive film of Fe–10Cr–3Si alloy, a main peak which was considered to correspond to Si^{4+} was observed at approximately 103 eV. The intensity of the peak at approximately 99.3 eV[33] corresponding to the metallic state was relatively low. The reverse tendency was observed in the interior. In the Cr $2p_{3/2,1/2}$ spectrum of the passive film of Fe–10Cr–3Al alloy, two peaks at 577 eV and 587 eV corresponding to Cr^{3+} on the surface of the film shifted to those at 574 eV and 583 eV corresponding to the metallic state after sputtering for 270 s. In the case of Fe–10Cr–3Si alloy, two similar peaks were observed when the sputtering times were 30 s and 270 s. However, in sputtering for 150 s, the sift of

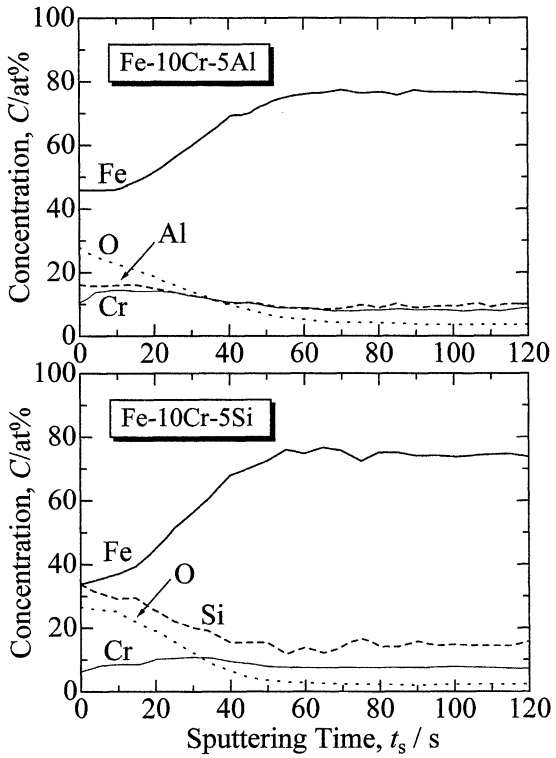

Fig. 11 AES depth profiles for the passive films formed on Fe–10Cr–5Al and Fe–10Cr–5Si alloys by passivation in 30 mass%HNO_3 solution at 303 K for 3.6 ks.

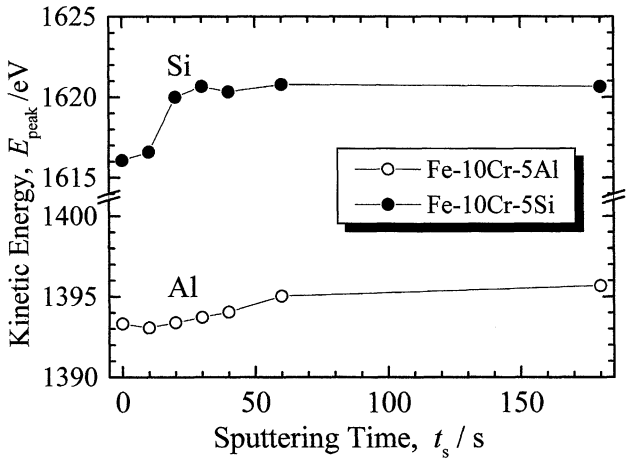

Fig. 12 Chemical shifts of kinetic energy of Al and Si obtained by AES depth analysis of Fe–10Cr–5Al and Fe–10Cr–5Si alloys.

these two peaks were little in the Fe–10Cr–3Al alloy, while the peaks were sifted to nearly the metallic state in the Fe–10Cr–3Si alloy. These observations suggest that the passive film mainly composed of Cr was thinner in the Fe–10Cr–3Si alloy than in the Fe–10Cr–3Al alloy. In the Mo $3d_{5/2,3/2}$ spectrum, a main peak at 232 eV and minor peak corresponding to metallic state at 228 eV were observed on the surface. In the interior, peaks shifted to 228 eV and 231 eV. Although no region where Mo was concentrated was observed by AES analyses, the height of the Mo peaks increased in the interior according to XPS analyses. The decrease of the concentration of Mo is possibly due to the concentration of Cr, Al and Si on the surface. This cause us to speculate that a large amount of Mo does not exist in the passive film in which Cr and Al or Cr

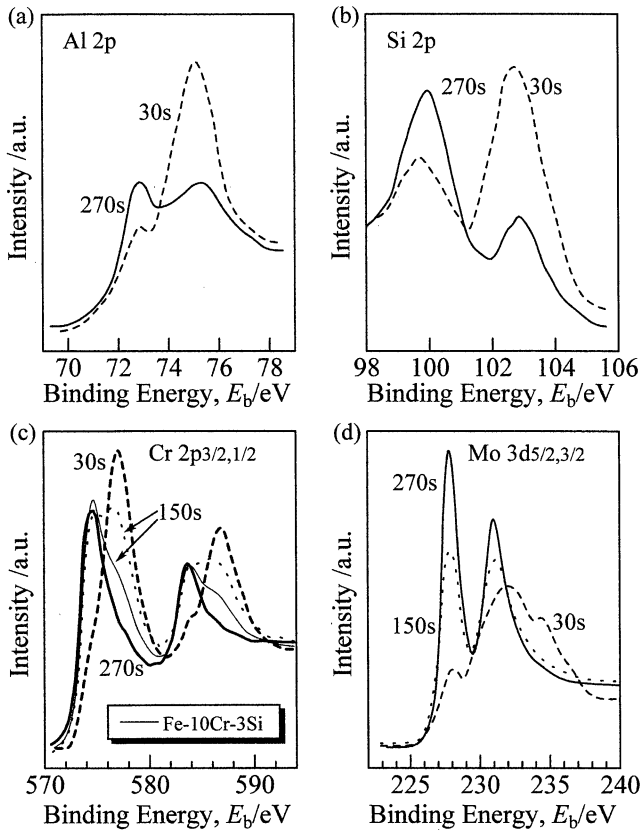

Fig. 13 Chages in XPS spectra with sputtering time for the passive films formed on Fe–10Cr–3Al (a) (c), Fe–10Cr–3Si (b) and Fe–10Cr–2Mo (d) alloys by passivation in 30 mass%HNO_3 solution at 303 K for 3.6 ks.

and Si are concentrated, but a high concentration of Mo exists on the matrix side.[34] We also analyzed the oxygen 1s spectrum and observed two peaks at 530.5 eV and 532 eV on the surface of the alloys. These peaks correspond to oxide O^{2-} (M–O bonding) and hydroxide OH^- (M–OH bonding),[32] respectively. In the interior, only a peak corresponding to oxide[35] at approximately 530.5 eV was detected, in agreement with the finding that more oxides were observed in the interior of passive films.

Schematic illustrations of the enrichment of alloying elements in the passive film are shown in Fig. 14. It will be pointed out that the passive film of the Al-added alloy forms a monolayer where Cr coexisted with Al, on the other hand, that of the Si-added alloy forms the two-layers structure where Si concentrated in the outer layer and Cr concentrated in the inner layer. The potential decay of the passive film, shown in Fig. 7, behaved in the two-step manner in the Fe–10Cr alloy containing Si. It is consistent with the passive film model which was induced by the analytical data of AES and XPS. As for the Mo-added alloys, the two-step decay of the passive film was also observed. Moreover, the time keeping the passive state of the second step was the longest in the case of the combined addition of Si and Mo. Although the enrichment of Mo by AES could not be detected, the compositional change of the passive film during potential decay process should be necessary to examine in detail in the future study.

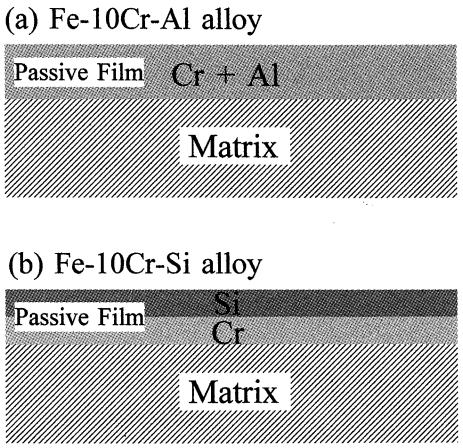

Fig. 14 Schematic illustrations of enrichment of Cr, Al, and Si in the passive films of Fe–10Cr–Al (a) and Fe–10Cr–Si (b) alloys.

4. Conclusions

Effects of Al, Si and Mo on the anodic polarization curves and pitting corrosion of Fe–10Cr alloys were studied. Potential decay curves were measured in order to evaluate the stability of the passive films on these alloys. The analysis of the chemical composition of the passive film was also carried out by AES and XPS. Results obtained in this study are as follows.

(1) The addition of Mo was very beneficial to decrease the critical passivation current density of Fe–10Cr alloys that contained Al and Si. The passive current density decreased with addition of 2%Mo to Fe–10Cr–3Si alloy, while it increased in Fe–10Cr–3Al alloy. The pitting potential shifted to noble direction except for Fe–10Cr–3Al–3Si–2Mo alloy when Mo was added. Laves phase (Fe_2Mo) was precipitated in the Fe–10Cr–3Al–3Si–2Mo alloy. It seems that Mo-depleted zone was formed locally, and the microstructure became inhomogeneous.

(2) The potential decay time of the passive film was increased by the addition of Al, Si and Mo to Fe–10Cr alloys. Two step potential decay curves were obtained in alloys contained Si and Mo, and this behavior of the decay curve was shown more clearly in Fe–10Cr–3Si–2Mo alloy.

(3) The results of AES and XPS analysis indicated that Cr and Al concentrated in the passive film of Fe–10Cr–Al alloy. In the case of Fe–10Cr–Si alloy, Si concentrated in the surface layer of the film and Cr did in the inner layer of the film. The confirmation was not possible for the enrichment of Mo in the passive film.

Acknowledgements

The authors acknowledge Dr. Michio Okabe of Research and Development Lab., Daido Steel Co. for preparation of the alloys tested. The authors also express their sincere thanks to Mr. Akio Ito of Research and Development Lab., Daido Steel Co for his experimental work of AES and XPS.

REFERENCES

1) K. Hio, M. Tsutsui and Y. Hosoi: Corrosion **55** (1999) 822–824.

2) K. Hio, Y. Hosoi, M. Tsutsui and M. Okabe: J. Japan Inst. Metals **63** (1999) 1248–1254.
3) M. A. Streicher: Corrosion **30** (1974) 77–91.
4) H. Ogawa, H. Omata, I. Itoh and H. Okada: Corrosion **34** (1978) 52–60.
5) A. P. Bond: J. Electrochem. Soc. **120** (1973) 603–606.
6) H. Ogawa, I. Itoh, M. Nakada, Y. Hosoi and H. Okada: TETSU-TO-HAGANE **63** (1977) 605–613.
7) N. J. E. Dowling, Y.-H. Kim, S.-K. Ahn and Y.-D. Lee: Corrosion **55** (1999) 187–199.
8) R. P. Frankenthal: J. Electrochem. Soc. **116** (1969) 1646–1651.
9) G. Okamoto: Corros. Sci. **13** (1973) 471–489.
10) N. Sato: Corros. Sci. **31** (1990) 1–19.
11) K. Sugimoto: Bulletin of the Japan Institute of Metals **24** (1985) 754–761.
12) G. Okamoto, K. Tachibana, T. Shibata and K. Hoshino: J. Japan Inst. Metals **38** (1974) 117–124.
13) H. Ogawa, I. Itoh, M. Nakada, Y. Hosoi and H. Okada: SEITETSU KENKYU No. 292 (1977) 9–20.
14) S. Haupt and H.-H. Strehblow: Corros. Sci. **37** (1995) 43–54.
15) K. Asami, K. Hashimoto and S. Shimodaira: Corros. Sci. **18** (1978) 151–160.
16) N. Ohtani: Bulletin of the Japan Institute of Metals **18** (1979) 547–551.
17) E. A. Lizlovs and A. P. Bond: J. Electrochem. Soc. **116** (1969) 574–579.
18) M. B. Rockel: Corrosion **29** (1973) 393–396.
19) T. Tsuru: Mater. Sci. Eng. **A146** (1991) 1–14.
20) J. W. Johnson, C. H. Chi, C. K. Chen and W. J. James: Corrosion **26** (1970) 238–242.
21) M. Seo, N. Sato and N. Sato: Bosyoku-Gijutsu **29** (1980) 281–289.
22) T. Nakamura and S. Haruyama: DENKI KAGAKU **48** (1980) 406–411.
23) K. Sugimoto and Y. Sawada: Corrosion **32** (1976) 347–352.
24) T. Kodama and J. R. Ambrose: Corrosion **33** (1977) 155–161.
25) S. Tsujikawa: *BOSHOKU-GIJUTSU-BINRAN*, ed. by T. Hisamatsu (Japan Society of Corrosion Engineering, Nikkan Kogyo Shinbunsha, Tokyo, 1986) pp. 32–36.
26) K. Shiobara and S. Morioka: J. Japan Inst. Metals **36** (1972) 385–392.
27) TDB-SSOL Data Base.
28) A. Iseda, H. Teranishi and K. Yoshikawa: TETSU-TO-HAGANE **76** (1990) 2190–2197.
29) K. Miyahara, J.-H. Hwang, Y. Shimoide, T. Iwamoto and Y. Hosoi: J. Japan Inst. Metals **59** (1995) 512–518.
30) A. E. Yaniv, J. B. Lumsden and R. W. Staehle: J. Electrochem. Soc. **124** (1977) 490–496.
31) R. Berneron, J. C. Charbonnier, R. Namdar-Irani and J. Manenc: Corros. Sci. **20** (1980) 899–907.
32) Y. Zhang, X. Zhu and S. Zhong: Steel Res. **64** (1993) 564–569.
33) J. F. Moulder, W. F. Stickle, P. E. Sobol and K. D. Bomben: *Handbook of X-ray Photoelectron Spectroscopy*, (Perkin-Elmer Corporation, Minnesota, 1992) pp. 54–57.
34) N. Hara: The 104th FUSHOKUBOSHOKU SHINPOJIUMU SHIRYO, ed. by T. Misawa (Japan Society of Corrosion Engineering, 1995) pp. 39–45.
35) K. Sugimoto: TETSU-TO-HAGANE **70** (1984) 637–649.